Chinese Chemical Letters 36 (2025) 110428

Contents lists available at ScienceDirect

Chinese Chemical Letters

journal homepage: www.elsevier.com/locate/cclet

Fe^{3+} ion quantification with reusable bioinspired nanopores

Yanqiong Wang[a], Yaqi Hou[a,*], Fengwei Huo[a], Xu Hou[b,c,d,e,f]

[a] Institute of Flexible Electronics (IFE, Future Technologies), Xiang'an Campus, Xiamen University, Xiamen 361102, China
[b] State Key Laboratory of Physical Chemistry of Solid Surfaces, College of Chemistry and Chemical Engineering, Xiamen University, Xiamen 361005, China
[c] Institute of Artificial Intelligence, Xiamen University, Xiamen 361005, China
[d] Department of Physics, Research Institute for Biomimetics and Soft Matter, Fujian Provincial Key Laboratory for Soft Materials Research, Jiujiang Research Institute, College of Physical Science and Technology, Xiamen University, Xiamen 361005, China
[e] Innovation Laboratory for Sciences and Technologies of Energy Materials of Fujian Province (IKKEM), Xiamen 361102, China
[f] Engineering Research Center of Electrochemical Technologies of Ministry of Education, Xiamen University, Xiamen 361005, China

ARTICLE INFO

Article history:
Received 20 June 2024
Revised 4 September 2024
Accepted 6 September 2024
Available online 7 September 2024

Keywords:
Bioinspired nanopores
Fe^{3+} ion quantification
Chemical binding affinity
Tannic acid
Reusability

ABSTRACT

Excessive Fe^{3+} ion concentrations in wastewater pose a long-standing threat to human health. Achieving low-cost, high-efficiency quantification of Fe^{3+} ion concentration in unknown solutions can guide environmental management decisions and optimize water treatment processes. In this study, by leveraging the rapid, real-time detection capabilities of nanopores and the specific chemical binding affinity of tannic acid to Fe^{3+}, a linear relationship between the ion current and Fe^{3+} ion concentration was established. Utilizing this linear relationship, quantification of Fe^{3+} ion concentration in unknown solutions was achieved. Furthermore, ethylenediaminetetraacetic acid disodium salt was employed to displace Fe^{3+} from the nanopores, allowing them to be restored to their initial conditions and reused for Fe^{3+} ion quantification. The reusable bioinspired nanopores remain functional over 330 days of storage. This recycling capability and the long-term stability of the nanopores contribute to a significant reduction in costs. This study provides a strategy for the quantification of unknown Fe^{3+} concentration using nanopores, with potential applications in environmental assessment, health monitoring, and so forth.

As the chemical industry flourishes, improper management of agricultural pollution, industrial wastewater, and urban sewage has significantly contaminated water resources with various metal ions. This contamination adversely affects biological systems and the ecological environment [1,2]. Among these metal ions, Fe^{3+} is one of the most crucial and prevalent metal ions in the ecosystem. Chronic exposure to excessive Fe^{3+} in water can result in increased iron load, posing a risk to human health [3-5]. Consequently, the detection and quantitative analysis of Fe^{3+} in the environment and organisms, supported by accurate data, can provide guidance for environmental assessment, food safety, health monitoring, clinical drug testing, and water treatment processes [6-10]. Hence, quantification of Fe^{3+} ion concentration in water environments is especially crucial.

Currently, several different strategies can be employed for the quantification of Fe^{3+} content in environmental water or within organisms. One of these strategies utilizes fluorescence or spectroscopic probes [11-21]. Through chelation or redox reactions between the molecules modified on fluorescence or spectroscopic probes and the Fe^{3+} ions, the fluorescence or the specific spectral intensity of the modified molecules changes, thereby achieving the quantification of Fe^{3+}. Alternatively, portable fluorescent paper can be used to detect Fe^{3+} by visually observing the color change on the fluorescent paper [22,23]. Electrochemical methods can be employed for Fe^{3+} detection by testing the redox reactions between nanocluster particles and Fe^{3+} [24,25]. Additionally, differential pulse voltammetry (DPV) can be used for the quantification of Fe^{3+} by measuring the changes in properties such as the surface double layer. Fe^{3+} concentrations can also be calculated by measuring absorbance changes and normalizing the results using spectrophotometric methods [26]. Furthermore, inductively coupled plasma mass spectrometry (ICP-MS) or inductively coupled plasma optical emission spectrometry (ICP-OES) can be employed for the quantification of Fe^{3+} through imaging and quantitative analysis [27,28]. However, in practical applications, these methods require the use of relatively expensive instruments such as fluorescence spectrometers, ICP-MS, or ICP-OES. Moreover, testing devices such as fluorescent test papers are often disposable. These approaches not only incur higher operational costs but also involve complex procedural and data analysis steps [29]. These fac-

* Corresponding author.
E-mail address: ifeyqhou@xmu.edu.cn (Y. Hou).

https://doi.org/10.1016/j.cclet.2024.110428
1001-8417/

tors limit the development of these methods for practical applications to some extent. Therefore, it is essential to develop a cost-effective, long-term functional, and rapid method for the quantification of Fe^{3+}.

The detection and sensing of substances using bioinspired nanopores has been rapidly advancing [30-32]. Combining bioinspired nanopore ion sensing with electrochemical techniques involves designing modified molecules and their interface roles on the inner surface of bioinspired nanopores [33-36]. The modified molecules can alter the charge on the inner surface of the bioinspired nanopores and interact with the detected ions through coordination or chelation. This alters the electrostatic, hydrogen bonding, and other interactions between the bioinspired nanopore surface and the detected ions, leading to changes in ion conductivity within the nanopores, which allow for the detection of specific ions. These current changes can be precisely measured using electrochemical methods, and the subsequent data analysis is not complex [37-39]. Previous attempts have demonstrated that tailoring the types of modified molecules on the inner surface of nanopores allows for regulating the interactions with Fe^{3+}, thereby influencing the ion current in the nanopores [39-44]. However, although these efforts enable detection of the presence of Fe^{3+} through nanopores, quantification of Fe^{3+} ion concentration using nanopores remains challenging.

Tannic acid (TA), a mixture of polygalloyl glucose molecules with different degrees of esterification, possesses polyphenol functional groups that can specifically interact with Fe^{3+} ions [45-47], as shown in Fig. S1 (Supporting information). Here, TA is adopted to build the TA-modified nanopores. The polyphenol structural fragments within TA molecules show differential binding affinities for various metal ions, and under specific pH conditions, they exhibit significantly stronger chemical coordination with Fe^{3+} ions. This strong affinity alters the surface charge of the nanopores, affects the thickness of the electric double layer within the nanopores, and significantly changes the ion current through nanopores. Meanwhile, we found that the equilibrium ion current (I_{eq}) in nanopores is linearly related to the concentrations of Fe^{3+} ($c_{Fe^{3+}}$) in the tested solutions. Thus, by measuring the ion current of a Fe^{3+}-containing solution passing through the TA-modified nanopores and correlating it to the linear relationship between I_{eq} and $c_{Fe^{3+}}$, quantification of Fe^{3+} ion concentration in the solution can be achieved. After detection, the introduction of ethylenediaminetetraacetic acid disodium salt (EDTA-2Na), which has a higher binding affinity with Fe^{3+}, can displace the Fe^{3+} bound to TA within the nanopores. This restoration allows for the repeated use of the nanopores for quantification of unknown Fe^{3+} ion concentrations, thereby reducing testing costs. This work not only enables rapid and efficient detection of target analytes, but also provides ease of operation, low cost, significant economic and practical value for the quantification of Fe^{3+}, demonstrating promising applications in fields such as environmental assessment, health monitoring, and beyond.

In this work, a single glass nanopore was first prepared using the bench-top method [39,48], and then functionalized with TA molecules. As depicted in Fig. S2 (Supporting information), (3-aminopropyl)triethoxysilane (APTES), which terminates with an amino group, was first modified on the nanopore. Subsequently, TA modified the reusable bioinspired nanopores through electrostatic interactions and hydrogen bonding between the trihydroxy phenolic groups of TA and the amino groups of APTES. To compare the changes in the properties of the glass surface before and after modification, atomic force microscopy (AFM) and contact angle characterization were performed on glass slides that underwent the same modification process. The bare glass surface is relatively smooth; however, after modification with APTES and TA molecules, the roughness of the glass surface increases (Fig. S2). The modified molecules adhere to the glass surface and remain stable even after washing with deionized water, indicating that the modified molecules have excellent stability. As shown in Fig. S3 (Supporting information), the bare glass slide has a contact angle of 27.6°, which increases to 79.0° after APTES modification and decreases to 42.2° following TA modification. These changes in contact angles confirm the success of the modification. Fig. 1a shows a schematic diagram of the testing set of the bioinspired nanopores. The Fe^{3+} ion current passing through the nanopore is tested. Compared to other metal ions, the interaction distance between TA fragments and Fe^{3+} is shorter, and the interaction force is stronger, laying the foundation for the quantification of Fe^{3+}. Meanwhile, *I-t* tests were conducted on solutions with varying concentrations of Fe^{3+} using TA-modified glass nanopores. By continuously applying voltage, it was found that the ion current in the nanopores gradually reached an equilibrium ion current (I_{eq}) corresponding to different Fe^{3+} ion concentrations. Additionally, the magnitude of this I_{eq} value is linearly related to $c_{Fe^{3+}}$ in the solution. Based on this linear relationship, the quantification of Fe^{3+} ions can be determined only by conducting an *I-t* test. For instance, as depicted in Fig. 1b, when the equilibrium ion current is I_{eq1} in the *I-t* test, the corresponding Fe^{3+} ion concentration c_1 can be deduced from the I_{eq}-$c_{Fe^{3+}}$ linear relationship. Similarly, when the equilibrium ion current is I_{eq2}, the corresponding Fe^{3+} ion concentration in the solution is identified as c_2. Furthermore, the nanopores can be restored to their initial condition by being cleaned with EDTA-2Na after binding with Fe^{3+} ions for multiple times (Fig. 1c), demonstrating the reusability for Fe^{3+} ion quantification.

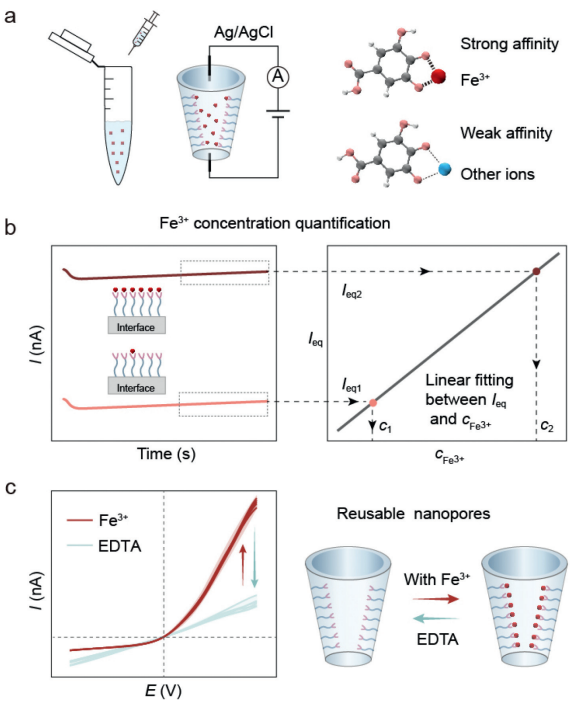

Fig. 1. Quantification of Fe^{3+} ions by reusable bioinspired nanopores. (a) The schematic of the testing set and specific binding affinity of TA molecular fragments with Fe^{3+}. (b) Quantification of Fe^{3+} ion concentration in an unknown solution. The concentrations of Fe^{3+} in the solution can be quickly obtained through *I-t* testing by correlating the equilibrium ion current (I_{eq}) from solutions to their respective Fe^{3+} ion concentrations ($c_{Fe^{3+}}$) based on the I_{eq}-$c_{Fe^{3+}}$ linear relationship. (c) Reusable TA-modified nanopores showing reversible interactions between EDTA-Fe^{3+} and TA-Fe^{3+}.

I-V tests were conducted on 1.0 mmol/L KCl solutions mixed with various metal ions, including 0.1 mmol/L solutions of LiCl, NaCl, $MgCl_2$, $CuCl_2$, $AlCl_3$, and $FeCl_3$, under different pH conditions. The surface charge of TA-modified nanopores varies under differ-

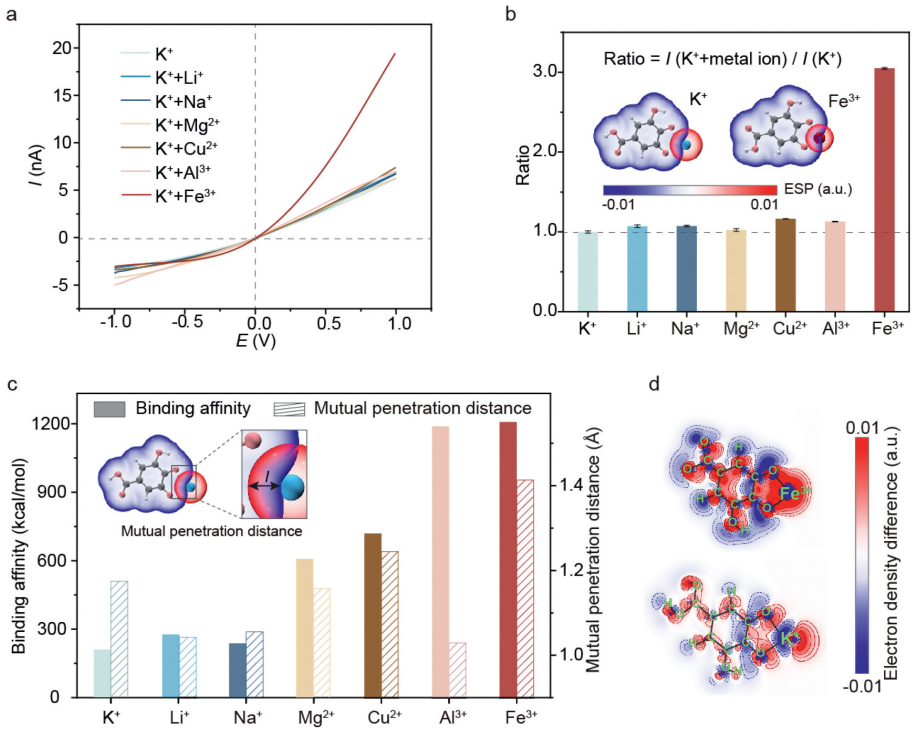

Fig. 2. Specific interaction between Fe^{3+} and TA-modified nanopores. (a) *I-V* curves (from −1 V to +1 V) of TA-modified nanopores in various ion solutions (pH 5–6), with a 1.0 mmol/L KCl base solution and 0.1 mmol/L other solutions of different metal ions. (b) At +1 V, the current ratio of solutions with added metal ions to the base KCl solution. Inset: electrostatic potential mapped van der Waals surface ($\rho = 0.001$ a.u. isosurface) of TA-K^+ and TA-Fe^{3+} complexes. (c) The absolute values of the binding energies ($|E_{bind}|$) and mutual penetration distance (l) between TA and various ions at optimized structures. (d) Electron density difference (EDD) map caused by interactions between TA fragment and ions.

ent pH conditions, as shown in Fig. S4 (Supporting information), affecting the *I-V* curves for each solution. When the pH is 4, TA-modified nanopores are positively charged, resulting in a weaker binding ability with metal ions. The current of the solution containing Fe^{3+} is higher than that of solutions mixed with other ions (Fig. S5a in Supporting information). When the pH range is 9–10, the surface charge of TA-modified nanopores shifts from positive to negative, reversing the ion rectification phenomenon. Under this condition, it is difficult to distinguish between solutions containing Fe^{3+} and those containing other ions based on the magnitude of the ion current (Fig. S5b in Supporting information).

When the pH is 5–6, the *I-V* curve changes for different solutions of metal ions are generally not significant, except for the Fe^{3+} ion solution. In the presence of Fe^{3+}, the *I-V* curve of the KCl solution exhibits a noticeable difference in current values as shown in Fig. 2a. This significant difference, demonstrating the specificity between TA and Fe^{3+}, provides a foundation for the quantification of Fe^{3+}. Further comparisons were made of the current magnitude of KCl solutions containing various metal ions at a voltage of +1 V. As shown in Fig. 2b, the ratio of the current value of KCl solutions containing different metal ions ($I_{K^+ + metal\ ion}$) to the current value of the solution containing only KCl (I_{K^+}) at +1 V is displayed. One can see that the ratio for the solution containing Fe^{3+} to the KCl solution is about 3, whereas the ratios for other metal ions are close to 1. Therefore, at a pH of 5–6, the specificity between TA and Fe^{3+} is the most pronounced, enabling the recognition of Fe^{3+}.

To delve into the interactions between TA molecules and different ions, calculations based on density functional theory (DFT) were carried out. The primary TA molecular fragment involved in these interactions between TA and ions is the polyphenol, which tends to deprotonate two phenolic hydroxyl groups at a pH of approximately 4–5, resulting in two negative charges on the TA fragment [45]. Therefore, we selected polyphenol structural fragments carrying two negative charges to construct TA-ion complex models and calculate their interactions with various ions, including Li^+, Na^+, K^+, Mg^{2+}, Cu^{2+}, Al^{3+}, and Fe^{3+}. To find the most stable structures of the TA-ion complexes, 50 original conformations of TA-ion adsorption clusters for each ion were generated using Molclus [49]. Then all the original TA-ion complexes were optimized using the PBE0 method [50] in conjunction with the def1TZVP basis set [51,52]. The TA-ion complex structures with the lowest energies for each kind of ion were selected as the optimized structures.

The binding energy (E_{bind}) represents the change in electronic energy during the formation of TA fragment-ion complexes from separated TA fragment and ions. The E_{bind} was calculated at the B3LYP/def2TZVP [53,54] level with Grimme's D3BJ dispersion [55] depending on the following equation (Eq. 1):

$$E_{bind} = E_{TA-ion} - (E_{TA} + E_{ion}) \quad (1)$$

The electrostatic potential (ESP) plays a crucial role in determining weak interactions. Typically, the isosurface of the electron density, $\rho = 0.001$ a.u., is employed to define the molecular van der Waals (vdW) surface [56]. The ESP on the vdW surface is often investigated because it significantly influences intermolecular electrostatic interactions.

To compare the interactions between different ions and TA fragments, the ESP-colored vdW surface maps of TA-K^+ and TA-Fe^{3+} complexes are shown in the inset of Fig. 2b. The ESP-mapped vdW surfaces of the TA fragments are depicted in blue, while those of the metal ions are depicted in red. From these depictions, it can be inferred that in the TA-ion complexes, the TA structural fragments exhibit negative ESP, while the positively charged ions display positive ESP. This difference in surface ESP facilitates the positive and negative electrostatic interactions between the TA fragments and metal ions. To further quantitatively represent the strength of these electrostatic interactions, Fig. 2c displays the absolute values of the

binding energies ($|E_{bind}|$) between TA and various ions. In fact, all ions exhibit negative binding energies with TA fragments, indicating that the interactions are of an affinitive nature. The greater the magnitude of E_{bind}, the stronger the interaction between the ion and the TA fragment. Among all considered ions, Fe^{3+} exhibits the largest binding energy, inferring the strongest binding affinity among different ions.

The mutual penetration distance (l) between the molecular surfaces of TA fragments and ions was also calculated. As illustrated in the inset of Fig. 2c, l is defined as the distance at which the surfaces of the two fragments overlap. This distance l can quantitatively measure the strength of electrostatic interactions. It can be observed that as the positive charge of the ions increases, the overall l between TA and ion surfaces tends to increase, with Fe^{3+} exhibiting a significantly greater l than all other ions. By combining the binding energy E_{bind} and the penetration distance l, it can be concluded that the interaction between TA molecules and Fe^{3+} differs significantly from those with other ions, which is the root cause of Fe^{3+} exhibiting specificity in this context.

To further demonstrate the polarization effect of metal ions on the electron distribution in TA molecules, variations in electron distribution during the binding processes are depicted with 2D electron density difference (EDD) maps in Fig. 2d. The EDD, defined as $\Delta\rho = \rho_{TA\ -\ ion} - (\rho_{TA} + \rho_{ion})$, can vividly display the electron transfer and polarization caused by the interactions between TA fragments and ions. Regions where electron density ρ decreases are depicted in blue, while regions where electron density ρ increases are depicted in red. A comparison of the EDD maps for TA-K^+ and TA-Fe^{3+} reveals that the electron density around Fe^{3+} significantly increases upon interaction with TA fragment molecules, indicating that many electrons from the TA fragment molecules are attracted and polarized towards Fe^{3+}. In contrast, the polarization effect of K^+ on the electron density of TA fragment molecules is less pronounced. This strong electron polarization effect indirectly reflects the strong interaction between Fe^{3+} and TA molecules. The ESP and electron density were obtained and visualized using Multiwfn 3.8 (dev) [57]. The final complex molecular structures and calculated results were rendered by the VMD visualization program [58].

To further demonstrate that the significant increase in ion current in the Fe^{3+}-containing KCl solution is attributable to the specific binding of TA-modified with Fe^{3+}, the ion current of solutions mixed with different ions in bare glass nanopores were also tested (Fig. S6 in Supporting information). Due to the presence of silanol groups on the surface of bare glass slides, the surface charge varies under different pH conditions (Fig. S6a). When using bare glass nanopores without modification, as shown in Figs. S6b and c, the nanopores exhibit variations in current for Fe^{3+} at pH 4 and 5. However, compared to TA-modified nanopores, the differences caused by Fe^{3+} are significantly reduced. At pH 10, bare glass nanopores also exhibit a reversal of ion selectivity (Fig. S6d). However, the ion current of the solution containing Fe^{3+} is similar to that of other solutions and cannot be distinctly differentiated. A comparison was also made between TA-modified nanopores and bare glass nanopores before and after rinsing with a Fe^{3+}-containing solution. Testing was conducted using the base KCl solution. The TA-modified nanopores showed significant differences before and after rinsing with the Fe^{3+}-containing solution, indicating that TA binding with Fe^{3+} alters the surface charge density (Fig. S7a in Supporting information). For bare glass nanopores, as shown in Fig. S7b (Supporting information), the tests with the KCl solution both before and after rinsing with the Fe^{3+}-containing solution showed almost overlapping curves, indicating that bare nanopores do not bind with Fe^{3+}. This demonstrates the specificity between TA and Fe^{3+} and directly confirms that the significant changes in the *I-V* curves are attributable to the effect of the modified TA molecules.

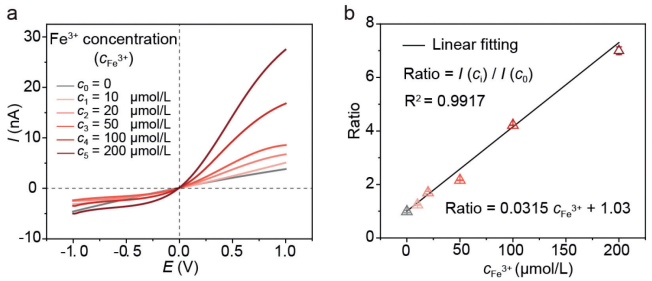

Fig. 3. Comparison of ion currents of KCl solutions containing different concentrations of Fe^{3+}. (a) *I-V* curves for Fe^{3+}-containing solutions with Fe^{3+} concentrations of 0, 10, 20, 50, 100, and 200 μmol/L. (b) At a voltage of +1 V, the ratio of the current values for solutions with different Fe^{3+} concentrations (I_{c_i}) to those without Fe^{3+} (I_{c_0}) demonstrates a linear relationship with Fe^{3+} concentration ($c_{Fe^{3+}}$).

It is worth noting that when testing unknown solutions, selecting a base solution and diluting unknown solutions strategically helps minimize interference from other ions, thereby enhancing the accuracy of the detection results. If the current of the base solution is too high, it may obscure the current changes of the Fe^{3+} ion-containing solution, thereby affecting the accuracy of the detection. Conversely, if the concentration of the base solution is too low, the current will be very small and susceptible to external interference, leading to an increase in the relative value of current fluctuations and consequently, the potential for increased error. Through theoretical calculations and experimental validation, it was determined that the solution of monovalent ions, which weakly bind with tannic acid, can meet the detection requirements. Therefore, this study selected KCl solution as the base solution.

Based on the above analysis, a pH range of 5–6 and a KCl base solution were selected because the specificity for Fe^{3+} is most pronounced under these conditions. *I-V* tests were conducted on solutions containing different concentrations of Fe^{3+}. As shown in Fig. 3a, using a 1 mmol/L KCl solution as the base solution, the current gradually increased at +1 V as the $c_{Fe^{3+}}$ increased. Fig. 3b illustrates the ratio of the current value of KCl solutions containing Fe^{3+} (I_{c_i}) to the current value of the base KCl solution without Fe^{3+} (I_{c_0}) at +1 V. The fitting of the current ratio with different $c_{Fe^{3+}}$ demonstrates a linear relationship: $Ratio = 0.0315c_{Fe^{3+}} + 1.03$, and $R^2 = 0.9917$. Therefore, based on the linear relationship between $c_{Fe^{3+}}$ and the current ratio, *I-V* tests can be used to achieve quantification of $c_{Fe^{3+}}$. The chosen concentration range for this detection method is set from 10 μmol/L to 200 μmol/L. To further assess the adaptability of this method to other base solutions, variations in the concentration of the KCl solution and other monovalent ion solutions were selected as base solutions. As illustrated in Figs. S8 and S9 (Supporting information), 0.5 mmol/L KCl and 1.0 mmol/L NaCl were chosen as base solutions for testing. Both of these results demonstrated a very good linear relationship, confirming that the method can potentially be expanded to include a broader range of monovalent metal ion solutions.

Fig. 4a shows the change in ion current over time for solutions with different concentrations of Fe^{3+}. As depicted in the inset of Fig. 4a, the current of the solution gradually approaches an equilibrium current (I_{eq}) over time. By analyzing the I_{eq} of solutions with different concentrations, it can be observed that the I_{eq} value increases as the $c_{Fe^{3+}}$ increases. A linear fit between I_{eq} and $c_{Fe^{3+}}$ was performed, as shown in Fig. 4b. The fitted curve is $I_{eq} = 0.1334c_{Fe^{3+}} + 3.97$, with $R^2 = 0.9949$. Therefore, by performing an *I-t* test on an unknown solution and then using the fitted curve of I_{eq} *versus* $c_{Fe^{3+}}$, the Fe^{3+} ion concentration of the un-

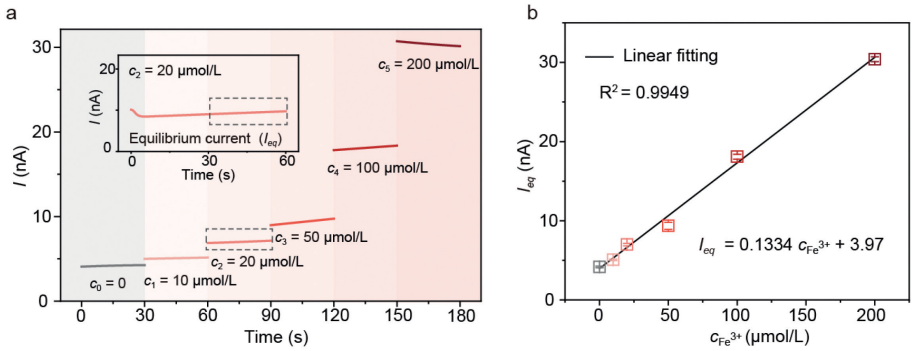

Fig. 4. Quantification of Fe^{3+} ion concentration using TA-modified reusable bioinspired nanopores. (a) The current measured for different concentrations of Fe^{3+} in TA-modified nanopores at a constant voltage (+1.0 V) over 60 s, shown in the inset. Between 30 s and 60 s, the ion current stabilizes, reaching an equilibrium current (I_{eq}). (b) Linear fit of the relationship between equilibrium current (I_{eq}) and Fe^{3+} ion concentration ($c_{Fe^{3+}}$).

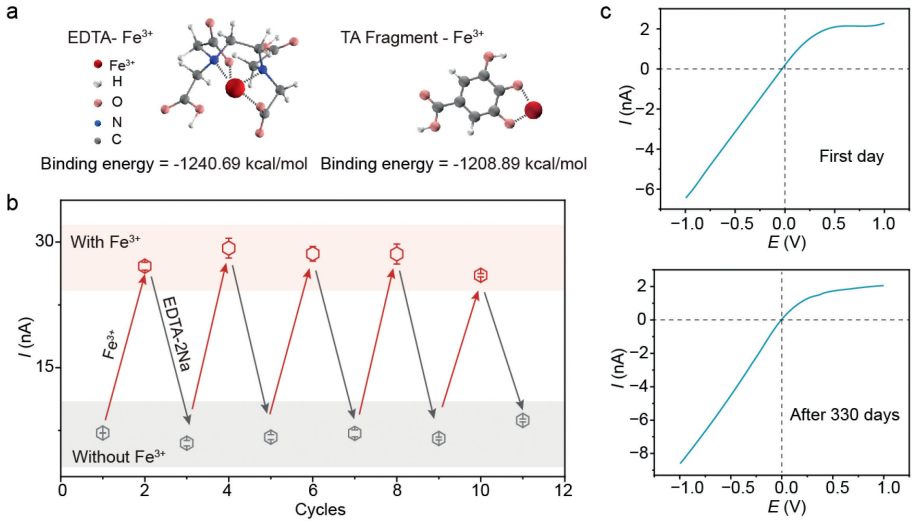

Fig. 5. Cycle and long-term functional stability of TA-modified nanopores. (a) Comparison of the binding energies between EDTA-Fe^{3+} and TA-Fe^{3+} complexes. (b) Cycle testing of TA-modified nanopores at +1 V and pH 5, in solutions with an Fe^{3+} ion concentration of 0.1 mmol/L or with EDTA-2Na. (c) Comparison of *I-V* curves tested on the first day and after 330 days using the same nanopore.

known solution can be obtained. This *I-t* testing method proves to be more practical and convenient in real-world applications compared to the previously described *I-V* testing approach.

To validate the cycle stability of nanopores for the quantification of unknown Fe^{3+} ion concentration, EDTA-2Na was used to clean the nanopores after testing. Owing to the stronger binding affinity of EDTA-2Na with Fe^{3+}, it can displace Fe^{3+} from the nanopores where it is bound to TA. To compare the binding energies of EDTA-2Na and TA with Fe^{3+}, DFT analyses were also conducted. Similar to the method used to calculate the E_{bind} between TA and Fe^{3+}, the interaction between Fe^{3+} and EDTA molecules was also calculated at the B3LYP/def2TZVP level (Fig. 5a). One can see that the E_{bind} between EDTA and Fe^{3+} (−1240.69 kcal/mol) is significantly higher than that between TA and Fe^{3+} (−1208.89 kcal/mol). Therefore, upon the introduction of EDTA molecules into the nanopores, Fe^{3+} preferentially binds to EDTA, thereby displacing Fe^{3+} from the TA-modified nanopores and restoring the nanopores to their initial condition.

The binding of Fe^{3+} to TA alters the channel ion current signal, enabling quantification of Fe^{3+}. Additionally, the ability of EDTA-2Na to restore the channel to its initial condition facilitates its reusability and test stability (Fig. 5b). This suggests that the nanopore system employed in this study can be repeatedly utilized for the quantification of Fe^{3+} ion concentration, further reducing the cost. The *I-V* curves in the cycle tests are shown in Fig. S10 (Supporting information). The significant differences in the curves before and after the presence and removal of Fe^{3+} also demonstrate the accuracy and reusability of the Fe^{3+} quantification system. Additionally, comparing the test results from the same glass nanopore on the first day and after 330 days of storage, no significant changes in ion current were observed, as shown in Fig. 5c. This indicates that the quantification function of the nanopores possesses long-term reliability and stability. Therefore, using nanopores can not only perform quantification of different $c_{Fe^{3+}}$ in solutions for multiple times but also ensure high stability over extended periods. Thus, the TA-modified glass nanopore offers stability, convenience, and cost-effectiveness in a system for quantification of Fe^{3+} in solutions.

In summary, we developed a reusable TA-modified nanopore system that specifically recognizes Fe^{3+} ions and can be used for the quantification of Fe^{3+} concentration, addressing some challenges in Fe^{3+} analysis, such as universality, portability, and affordability, thereby eliminating the dependency on expensive instruments. TA-modified nanopores utilize the specific interaction between TA molecules and Fe^{3+}. A linear relationship between Fe^{3+} ion concentration and detection current is established, making this method suitable for quantification of Fe^{3+} ion concentrations in unknown solutions. Furthermore, the nanopore device demonstrates exceptional stability, maintaining its functionality after 330 days of storage, which supports the sustainability and sig-

nificantly reduces the operational costs by reusing the nanopores. Therefore, this method for the quantification of Fe^{3+} not only offers benefits such as low cost, fast response, and high stability but also paves the way for advanced quantification applications, including environmental monitoring and real-time detection.

Declaration of competing interest

The authors declare that they have no known competing financial interests or personal relationships that could have appeared to influence the work reported in this paper.

CRediT authorship contribution statement

Yanqiong Wang: Writing – review & editing, Writing – original draft, Data curation. **Yaqi Hou:** Writing – review & editing, Formal analysis, Data curation. **Fengwei Huo:** Supervision, Funding acquisition. **Xu Hou:** Funding acquisition, Conceptualization.

Acknowledgments

This work was supported by the National Natural Science Foundation of China (Nos. 52303380, 52025132, 52273305, 22205185, 21621091, 22021001, and 22121001), Fundamental Research Funds for the Central Universities (No. 20720240041), the 111 Project (Nos. B17027 and B16029), the National Science Foundation of Fujian Province of China (No. 2022J02059), the Science and Technology Projects of Innovation Laboratory for Sciences and Technologies of Energy Materials of Fujian Province (No. RD2022070601), and the New Cornerstone Science Foundation through the XPLORER PRIZE.

Supplementary materials

Supplementary material associated with this article can be found, in the online version, at doi:10.1016/j.cclet.2024.110428.

References

[1] D. Hou, D. O'Connor, A.D. Igalavithana, et al., Nat. Rev. Earth. Environ. 1 (2020) 366–381.
[2] Y. Liu, G. Li, F. Lu, et al., Biomed. Pharmacother. 168 (2023) 115728.
[3] H. Deng, C. Tian, Z. Gao, et al., Analyst 145 (2020) 4931–4936.
[4] C. Brugnara, Clin. Chem. 49 (2003) 1573–1578.
[5] T. Hirayama, H. Nagasawa, J. Clin. Biochem. Nutr. 60 (2017) 39–48.
[6] A. Quijano-Rubio, H.W. Yeh, J. Park, et al., Nature 591 (2021) 482–487.
[7] R. Pandey, D. Chang, M. Smieja, et al., Nat. Chem. 13 (2021) 895–901.
[8] O. Herud-Sikimić, A.C. Stiel, M. Kolb, et al., Nature 592 (2021) 768–772.
[9] H. Wang, L. Da, L. Yang, et al., J. Hazard. Mater. 392 (2020) 122506.
[10] M. Safarkhani, A. Aldhaher, G. Heidari, et al., Nano. Mater. Sci. 6 (2024) 263–283.
[11] H.H. Hammud, S. El Shazly, G. Sonji, N. Sonji, K.H. Bouhadir, Spectrochim. Acta A 150 (2015) 94–103.
[12] S.F. Chin, S.C. Tan, S.C. Pang, S.M. Ng, Opt. Mater. 73 (2017) 77–82.
[13] R. Lv, Z. Chen, X. Fu, et al., J. Solid. State Chem. 259 (2018) 67–72.
[14] J. Xu, J. Yang, Z. Wang, et al., Mater. Design 236 (2023) 112465.
[15] A.M. Senol, Y. Onganer, J. Photochem. Photobiol. A 424 (2022) 113655.
[16] T.A. Khattab, M.E. El-Naggar, M. Pannipara, et al., Int. J. Biol. Macromol. 202 (2022) 269–277.
[17] N. Duan, F. Guo, B. Deng, et al., Luminescence 37 (2022) 803–809.
[18] Y. Su, J. Yu, Y. Li, et al., Commun. Chem. 1 (2018) 12.
[19] Y. Zheng, Q. Zhou, Y. Yang, et al., Small 18 (2022) 2201223.
[20] P. Jia, L. Gao, Y. Zheng, et al., ACS Appl. Mater. Interfaces 13 (2021) 33546–33556.
[21] P. Jia, Z. Wang, Y. Zhang, et al., Spectrochim. Acta A 230 (2020) 118084.
[22] N. Idros, D. Chu, ACS Sens. 3 (2018) 1756–1764.
[23] M. He, Y. Xiao, Y. Wei, B. Zheng, RSC Adv. 13 (2023) 31720–31727.
[24] S. Cong, Z. Jiang, R. Zhang, et al., Anal. Chem. 94 (2022) 6695–6702.
[25] G. Alberti, C. Zanoni, S. Rovertoni, L.R. Magnaghi, R. Biesuz, Chemosensors 10 (2022) 214.
[26] G.L. Smith, A.A. Reutovich, A.K. Srivastava, et al., J. Inorg. Biochem. 220 (2021) 111460.
[27] N. Stadler, R.A. Lindner, M.J. Davies, Arterioscl. Throm. Vas. 24 (2004) 949–954.
[28] C.R. Bhatt, D. Hartzler, D. McIntyre, Appl. Phys. B: Lasers O 130 (2023) 18.
[29] P. Arora, H. Zheng, S. Munusamy, et al., Biosens. Bioelectron. 251 (2024) e202400042.
[30] G.M. Roozbahani, X. Chen, Y. Zhang, et al., Small Methods 4 (2020) 2000266.
[31] Y. Hou, X. Hou, Science 373 (2021) 628–629.
[32] X. Hou, W. Guo, L. Jiang, Chem. Soc. Rev. 40 (2011) 2385–2401.
[33] Y. Hou, Q. Wang, S. Wang, et al., Chin. Chem. Lett. 33 (2022) 2155–2158.
[34] M. Wang, L. Zhou, Y. Hou, et al., Chin. Chem. Lett. 31 (2020) 1914–1918.
[35] Y. Hou, Y. Ye, Z. Du, et al., Chin. Chem. Lett. 31 (2020) 1640–1643.
[36] Y. Zhang, X. Hou, Natl. Sci. Open. 1 (2022) 20220035.
[37] Y. Liu, Y. Qian, L. Fu, et al., ACS Cent. Sci. 10 (2024) 469–476.
[38] R. Xu, Y. Kang, W. Zhang, B. Pan, X. Zhang, Nat. Commun. 14 (2023) 4907.
[39] K. Zhan, Z. Li, J. Chen, et al., Nano Today 33 (2020) 100868.
[40] C. Zhao, X. Li, L. Li, et al., Chem. Commun. 49 (2013) 9317–9319.
[41] M. Ali, S. Nasir, Q.H. Nguyen, et al., J. Am. Chem. Soc. 133 (2011) 17307–17314.
[42] B. Niu, K. Xiao, X. Huang, et al., ACS. Appl. Mater. Interfaces 10 (2018) 22632–22639.
[43] Y.C. Yang, J.P. Hsu, Langmuir 38 (2022) 11022–11032.
[44] X.T. Song, Y.D. Yin, G.R. Wu, M. Xu, Z.Y. Gu, Chin. J. Chem. 41 (2023) 2746–2757.
[45] H. Ejima, J.J. Richardson, K. Liang, et al., Science 341 (2013) 154–157.
[46] J. Guo, Y. Ping, H. Ejima, et al., Angew. Chem. Int. Ed. 53 (2014) 5546–5551.
[47] S. Kim, S. Philippot, S. Fontanay, et al., RSC Adv. 5 (2015) 90550–90558.
[48] Y. Ling, L. Yu, Z. Guo, et al., J. Am. Chem. Soc. 146 (2024) 14558–14565.
[49] T. Lu, Molclus Program, Version 1.12, Beijing Kein Research Center for Natural Science, China, 2016, https://www.keinsci.com/research/molclus.html.
[50] C. Adamo, V. Barone, J. Chem. Phys. 110 (1999) 6158–6170.
[51] A. Schäfer, H. Horn, R. Ahlrichs, J. Chem. Phys. 97 (1992) 2571–2577.
[52] A. Schäfer, C. Huber, R. Ahlrichs, J. Chem. Phys. 100 (1994) 5829–5835.
[53] F. Weigend, R. Ahlrichs, Phys. Chem. Chem. Phys. 7 (2005) 3297–3305.
[54] F. Weigend, Phys. Chem. Chem. Phys. 8 (2006) 1057–1065.
[55] S. Grimme, S. Ehrlich, L. Goerigk, J. Comput. Chem. 32 (2011) 1456–1465.
[56] R.F.W. Bader, M.T. Carroll, J.R. Cheeseman, C. Chang, J. Am. Chem. Soc. 109 (1987) 7968–7979.
[57] T. Lu, F. Chen, J. Comput. Chem. 33 (2011) 580–592.
[58] W. Humphrey, A. Dalke, K. Schulten, J. Mol. Graph. 14 (1996) 33–38.